BNL-44921
Informal Report

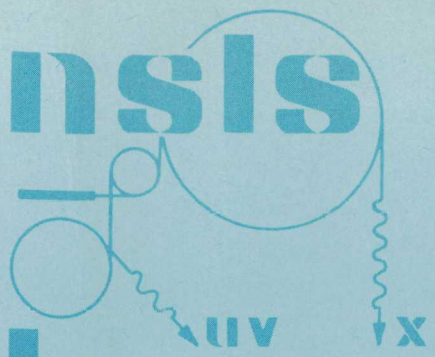

Magnetic Measurements of the NSLS Soft X-Ray Undulator

L. Solomon, J. Galayda and M. Kitamura

July 1990

NATIONAL SYNCHROTRON LIGHT SOURCE

BROOKHAVEN NATIONAL LABORATORY
ASSOCIATED UNIVERSITIES, INC.
Under Contract No. DE-AC02-76CH00016 with the
UNITED STATES DEPARTMENT OF ENERGY

Magnetic Measurements of the NSLS Soft X-Ray Undulator*

L. Solomon and J.Galayda

National Synchrotron Light Source

Brookhaven National Laboratory, Upton, New York 11973

M. Kitamura

Hitachi Research Laboratory, Hitachi, Ltd., Japan

The Soft X-Ray Undulator Magnet was installed in the X-Ray Ring (X1 beam line) at the National Synchrotron Light Source at Brookhaven National Laboratory in June 1988. Prior to its installation extensive magnetic measurements were performed at the NSLS Magnetic Measurements Lab in order to determine the operating values for the end corrector currents, the field quality, and the integrated multipoles associated with the magnet as a function of gap. This report is intended to summarize the results of these measurements.

A schematic of the SXU is shown in Figure 1. The iron poles are 18mm x 32mm x 86mm, and the Samarium Cobalt permanent magnet blocks are 22mm x 21mm x 110mm. In each of the magnet halves there are 76 slots, 70 of which were filled with two magnets per slot, and 6 of which were left empty (3 each on the upstream and downstream ends of the magnet). These slots were left empty in order to approximate an infinitely long magnet in the algorithm for the magnet

*This work was performed under the auspices of the U.S. Department of Energy.

block sorting. The magnet period is 80mm, and the gap range is 31 - 100mm, with field values of 3500 and 200 Gauss respectively. For this gap range the undulator parameter K, where K = 0.934 B(Tesla) λ(cm), ranges from 2.6 to 0.15.

Single Block Measurements.

The relative strength of each individual magnet was measured in a Helmholtz coil, where the integrated voltage generated as the magnet block slides down a chute is measured and is directly proportional to the magnetic strength. In this manner the average magnitude of two of the three orthogonal components of the magnetization, M_z and M_y, were measured for each block. In the assembled undulator the *major* magnetization, M_z was oriented along $\hat{z}$, and the *minor* component M_y, was along $\hat{y}$. For the SXU magnet blocks $M_y/M_z \leq 3\%$. This corresponds to an angular error in the block magnetization of $\approx 1.7°$.

To help determine specifically where the individual magnets should be located in the magnet halves, the magnetic field at the midplane of the undulator due to a single block (the *transfer function*) was measured prior to assembly of the two magnet halves. These transfer functions were used to specify the order of loading blocks in the magnet so as to optimize the electron beam trajectory. By translation symmetry the transfer functions for a block inserted in the middle of the magnet are correct for any block reasonably far from the end of the undulator. By reflection symmetry, a block with M_x and $M_y = 0$, inserted into a slot of an infinitely long undulator will produce a field with zero integral in the z direction, for any value of x and y(see figures 2 and 3). While additional measurements could have been done to obtain transfer functions for the slots near the end of the magnet, it was decided instead to leave the three poles at each end of the undula-

tor unexcited by magnet material. This had the added benefit of reducing the integrated field of the undulator to the level of that produced by errors in the strengths of the blocks. Electromagnets at the end were installed to correct the remaining field integral.

The transfer function was measured for a single block in the *high* position (closer to the magnet midplane) and *low* position (farther from the magnet midplane) in a magnet half, and for M_z oriented along $\hat{z}$ and along $\hat{y}$. To measure the *major* transfer function M_z was oriented along $\hat{z}$, and a steel plate was held over the magnet half. The plate set the boundary conditions and imposed midplane symmetry. The field with this geometry should be the same as if there was an identical magnet block in the identical position in the other magnet half, with a magnetization M_z along $-\hat{z}$. Therefore, the fields measured in this manner are actually twice the field due to a single magnet. In order to measure the *minor* transfer function an empty beam was used in place of the steel plate. These transfer functions are plotted in Figure 2. The first and second integrals associated with these fields are plotted in Figures 3 and 4 respectively. A notable feature of this data is that the integrated effect of the minor component of the magnet block further from the midplane is greater than that of the magnet nearer the midplane, though the magnitude of the midplane field is more strongly affected by the block nearer the midplane. This is due to the channeling of the magnetic flux through the steel backing plate.

The effect of a minor component along $\hat{x}$ was also measured, and in terms of peak field magnitude it has an affect which is $\approx$ 10% of that due to a minor component along $\hat{y}$ (Figure 5). Due to the different functional form associated with this field component, the integrated effect of this block error was $\approx$ 20% of that

due to M_y (Figures 6 and 7). Clearly, measurement of this transfer function enables the determination of vertical steering effects.

The M_y and M_z transfer functions were used to determine the placement of the 280 magnet blocks in the magnet beams. The optimal arrangement of magnet blocks minimizes the first and second integrals of the magnetic field, which are directly related to the angular deviation, Θ, and the linear displacement, X, respectively of the electron beam upon emerging from the insertion device i.e.

$$\Theta \approx \frac{1}{B\rho} \int_0^L B(z')dz' \tag{1}$$

$$X \approx \frac{1}{B\rho} \int_0^L dz \int_0^z B(z')dz' \tag{2}$$

where $B\rho$, the magnetic rigidity, is 8.3391 Tesla meters at 2.5 GeV, and L is the magnet length.

Assembled Magnet Measurements

The magnetic measurements of the assembled SXU magnet can be divided into two sections - the hall probe measurements and the long coil measurements. All measurements were taken with an IBM-AT operating with a Microport Unix system. C software was developed for the measurements and data analysis. The GPIB interface was used for all the instruments, and a serial port was used to handshake with the instruments through a Busmate (ICS Electronics).

For the hall probe measurements a Daedel-Compumotor 3000 controlled XY translator supported an F.W.Bell probe. The Hall voltage was determined with a Bell 8860 Field Detector, and was read with a Hewlett-Packard multimeter. The XY table was supported on a carriage which allowed z-motion (along the magnet length) of the hall probe through a stepping motor driven rack and pinion and a

Modulynx driver. The z position was determined with a Farrand Instruments transducer with an accuracy of ± 0.001 mm. This whole assembly was supported on an aluminum bed bolted onto an ≈ 14 foot long granite slab.

The long coil measurements utilized two coils supported on an ≈ 4.5 meter G10 tube (.750" outer diameter). The two coils were wound with 20 strand wire on two diameters of the G10 rod which were 90° from each other. Each coil resistance was ≈ 270 Ohms. During the long coil measurements the G10 tube was supported with aluminum outriggers fastened to the aluminum bed. The G10 rod was oriented so that one coil winding was initially in the x plane, to measure the dipole field, and the second coil winding was initially in the y plane, to measure the skew dipole field. The coil elevation was set with a Wild Optical Level. The G10 rod was flipped through 180° and the integrated voltage was read with an Hewlett-Packard multimeter. This was done for a series of x positions. The dependence of the dipole field on x, or equivalently the derivatives of the dipole field with respect to x are related to the higher order moments of the field, i.e.

$$B = B_0 + B'x + \frac{1}{2!}B''x^2 + \frac{1}{3!}B'''x^3 + \frac{1}{4!}B''''x^4 \qquad (3)$$

where B^0 is the dipole field, B' is the quadrupole field, B'' is the sextupole field, B''' is the octupole field and B'''' is the decapole field. The data as a function of x is fit to this form in order to ascertain the magnetic multipoles.

Results and Analysis - Hall Probe

The Hall probe was used to determine the magnetic field as a function of gap, or, equivalently, K as a function of gap. The data is presented in figure 8, and is fit to the expected form $B = B_0 / \sinh(\pi\ Gap/\lambda)$. The fit yields a value

B_0 =0.534, and is indicated by the solid line in Figure 8.

The hall probe measurements were also integrated to determine Θ, the angular displacement of the electron beam, and X, the electron beam trajectory, as a function of magnet gap (Eqs. 1 and 2). Hall probe measurements were taken at zero end corrector current, and also at the 'operating' current, or 'corrected' field, as determined with the long coil measurement results. The corrected angular displacement as a function of gap is shown in Figure 9. For clarity, the 40 mm trajectory is displaced by 0.5×10^{-3} radians from the 31 mm trajectory, the 50 mm trajectory is displaced by the same amount from the 40 mm trajectory, and so on. The corrected electron trajectories as a function of gap are shown in Figure 10. In this plot, the 40 mm trajectory is displaced by 0.1×10^{-4} meters from the 31 mm trajectory, and so on.

An exciting part of these measurements was experimental fine tuning of the field profile. By looking at the particle trajectories (figure 10) a kink is clearly evident at $\approx 1.6m$. By fitting the field data in the center of the magnet with a sinusoidal function it became clear that poles 44 and 46, which were positive poles, were a bit weak. In order to strengthen these poles we tried two techniques. One method was to attach 0.010" shim stock onto these poles in order to increase their strength. Alternatively, we also tried to decrease the strength of the negative pole 45, through the use of studs. The results we obtained were quite striking, and are shown in Figure 11. In order to obtain this data full magnet scans were taken for each of these configurations, and therefore was looks like a single plot up till $\approx$1.6 meters is actually three distinct plots which coincide impressively. These plots are the results of a double integration, and therefore all errors are amplified. To quantify this argument, consider the effect of a small

probe offset of .1 Gauss. This offset, which is completely undiscernible upon visual inspection of the field profile plots, integrates to 0.4 Gauss-meters, or 5×10^{-6} radians, and has a second integral of 1×10^{-5} meters. An effect of this order would be glaringly apparent in a plot such as Figure 11. Clearly both the studs and the shims had the desired effect, i.e. to remove the kink at $\approx$ 1.6m. Had we desired to permanently install one of these fixes in the magnet we would have also had to correct some of the other features in the trajectory.

Results and Analysis - Long Coil

Long coil measurements were carried out at magnet gaps of 31mm, 40mm, 50mm, 70mm, and 90mm, with the end corrector currents set at -10amps, 0 amps, and 10 amps. The integrated field was measured with the coil at the magnet center line, and displaced ± 10mm, ± 20mm, and ± 30mm off the centerline in the horizontal plane. The integrated voltage is a linear function of end corrector current (Figure 12-bottom) and is fit with a linear least squares fitting routine. All measurements were done as a function of z in increments of 10mm. through a range of 80mm., corresponding to the period of the magnet. The resulting data is fit to a sin function, and the offset is taken to be the net magnetic field integral (Figure 12 top). The integrals as a function of x and I are presented in Table 1. The table entries, which are in units of 10^{-6} radians, must be multiplied by the magnetic rigidity $B\rho$ to obtain Tesla meters.

In order to determine the current settings for the end corrector coils the field integral was measured in the X-ray ring at the location of the X1 insertion prior to actual installation. This field integral value was designated the 'desirable' magnet field integral, and the current at which this occured for a given gap was

determined (Figure 12 bottom). Table 5 has entries which indicate the chosen operating current, I_{oper}, as a function of gap.

A plot of the uncorrected field integral as a function of transverse position x is shown in Figure 13. This data was fit to Equation 3, to determine the higher magnetic multipoles, and the fit is indicated by the solid line. Table 2 tabulates the multipole field fit results in both the uncorrected(I=0.0) and the corrected(I=I_{oper}) magnet.

The long coil data for the skew dipole field, measured with the coil whose initial and final plane coincides with the y plane, is presented as a function of the transverse position x in Figure 14 and Table 3. The multipole analysis results are presented in Table 4.

A comparison of the Hall probe and the long coil results are presented in Table 5. Agreement between these two methods, which is strongly reliant upon careful and frequent zeroing of the Hall probe voltage, is $\leq 4\times10^{-6}$ radians, or $\approx$ 0.3 Gauss-meters, which corresponds to a small Hall probe offset of $\approx$ 0.08 Gauss, a fraction of the earth's field. Put into these terms, the agreement of these two methods is excellent.

The authors would like to acknowledge the contributions of G.Decker during the early stages of these measurements, and in the development of a sorting algorithm for the magnet blocks.

List of Figures

Figure 1 A sketch of the soft X-Ray undulator indicating the permanent magnet orientations and locations, and the coordinate system used in the text.

Figure 2 The measured single block transfer functions in the SXU for M_z // to $\hat{z}$ and $\hat{y}$. The nomenclature high means that the magnet block is closer to the magnet mid-plane, and low means that the magnet block is farther from the midplane.

Figure 3 The first integral of the single block transfer functions of Figure 2.

Figure 4 The second integral of the single block transfer functions of Figure 2.

Figure 5 The transfer function of the two minor components of the magnet block i.e. M_z // to $\hat{y}$ and M_z // to $\hat{x}$.

Figure 6 The first integral of the single block minor component transfer functions of Figure 5.

Figure 7 The second integral of the single block minor component transfer functions of Figure 5.

Figure 8 The undulator parameter K as a function of Gap

Figure 9 The magnetic field data at I=I_{oper} is integrated once to determine the angular displacement of the electron beam at magnet gaps of 90mm (I=-4.6amps), 70mm (I=-3.2amps), 50mm (I=-1.7amps), 40mm (I=-1.1amps), and 31mm (I=-0.65amps). For clarity the 40 mm trajectory is displaced by 0.5 $\times 10^{-3}$ radians from the 31 mm trajectory, the 50 mm trajectory is displaced by the same amount from the 40 mm trajectory, and so on.

Figure 10 The magnetic field data at I=I_{oper} is integrated twice to determine the elec-

tron trajectory at magnet gaps of 90mm (I=-4.6amps), 70mm (I=-3.2amps), 50mm (I=-1.7amps), 40mm (I=-1.1amps), and 31mm (I=-0.65amps). For clarity, the 40 mm trajectory is displaced by 0.1 $\times 10^{-4}$ meters from the 31 mm trajectory, the 50 mm trajectory is displaced by the same amount from the 40 mm trajectory, and so on.

Figure 11 The effect of a 0.010" shim on poles 44 and 46, and the effect of a pole 45 stud, at a 50mm gap.

Figure 12 Top The long coil field integral plotted as a function of long coil position, fit to a sine wave.

Figure 12 Bottom The long coil field integral plotted as a function of corrector current, with a linear least squares fit.

Figure 13 The long coil field integral at zero end corrector current, at 90, 70, 50, 40, and 31mm gaps as a function of X, with the fit to a fourth order polynomial indicated by the solid line.

Figure 14 The long coil skew field integral at 90, 70, 50, 40, and 31mm gaps as a function of X.

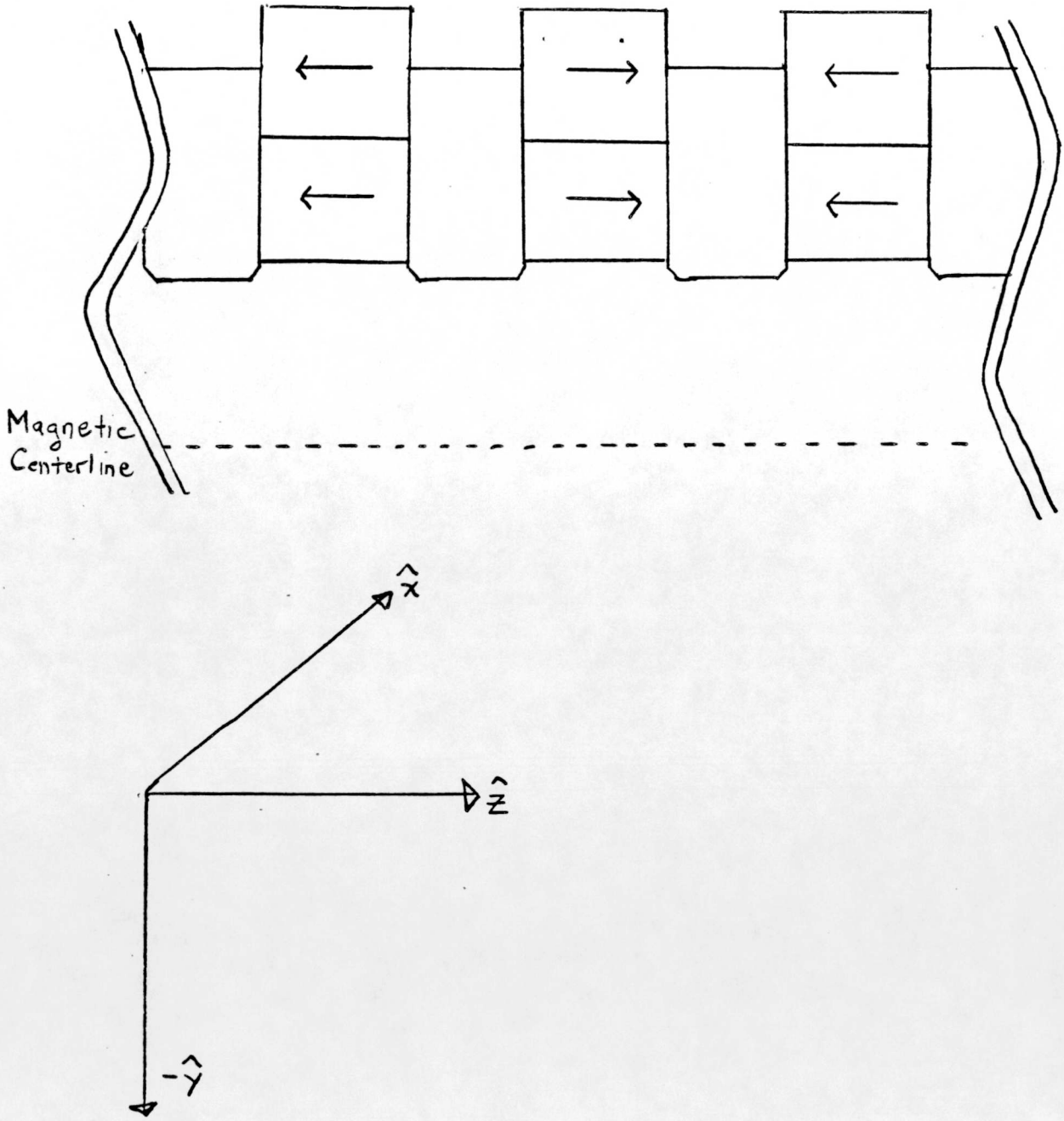

Figure 1 A sketch of the soft X-Ray undulator indicating the permanent magnet orientations and locations, and the coordinate system used in the text.

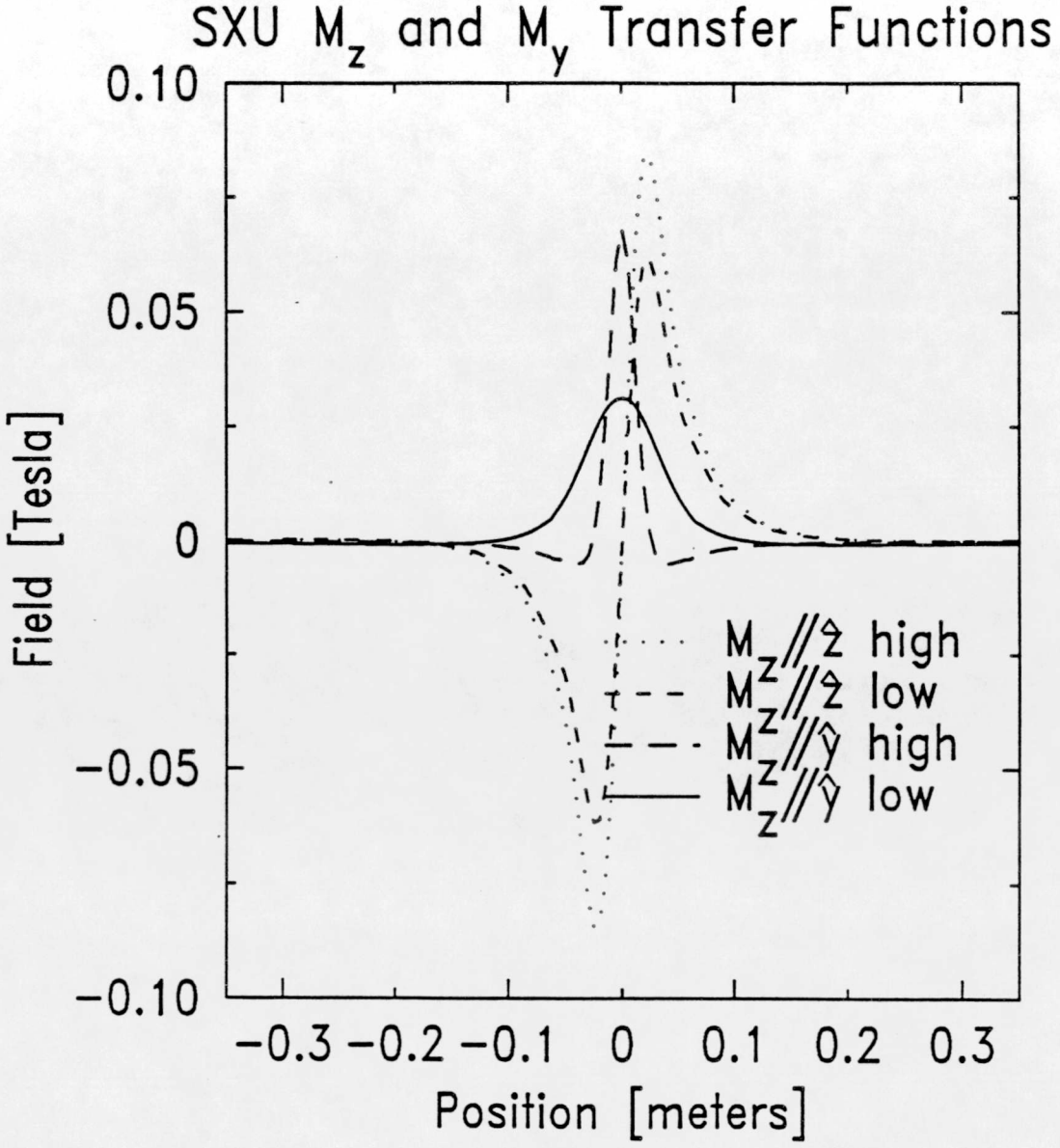

Figure 2 The measured single block transfer functions in the SXU for M_z // to $\hat{z}$ and $\hat{y}$. The nomenclature high means that the magnet block is closer to the magnet midplane, and low means that the magnet block is farther from the midplane.

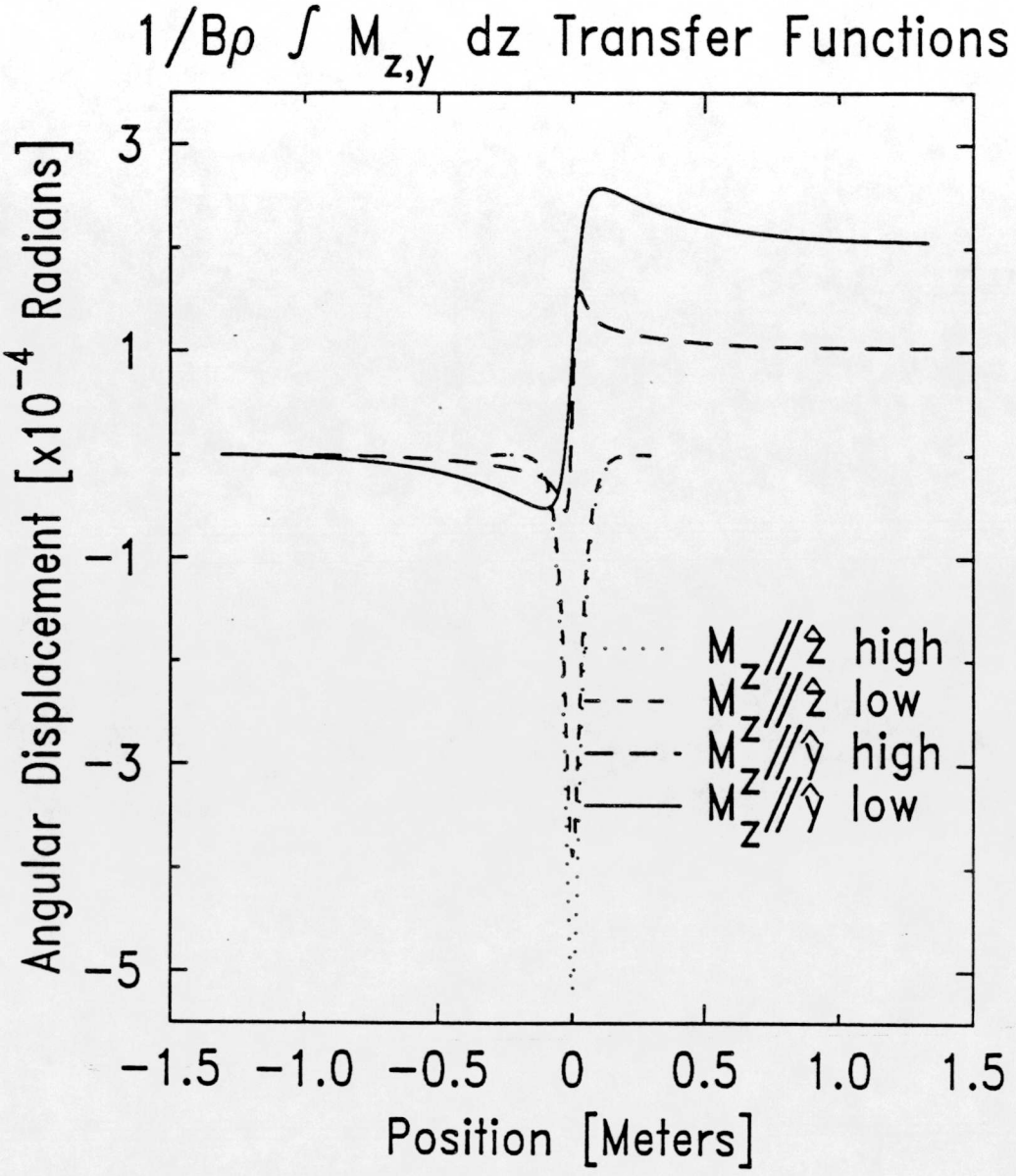

Figure 3 The first integral of the single block transfer functions of Figure 2.

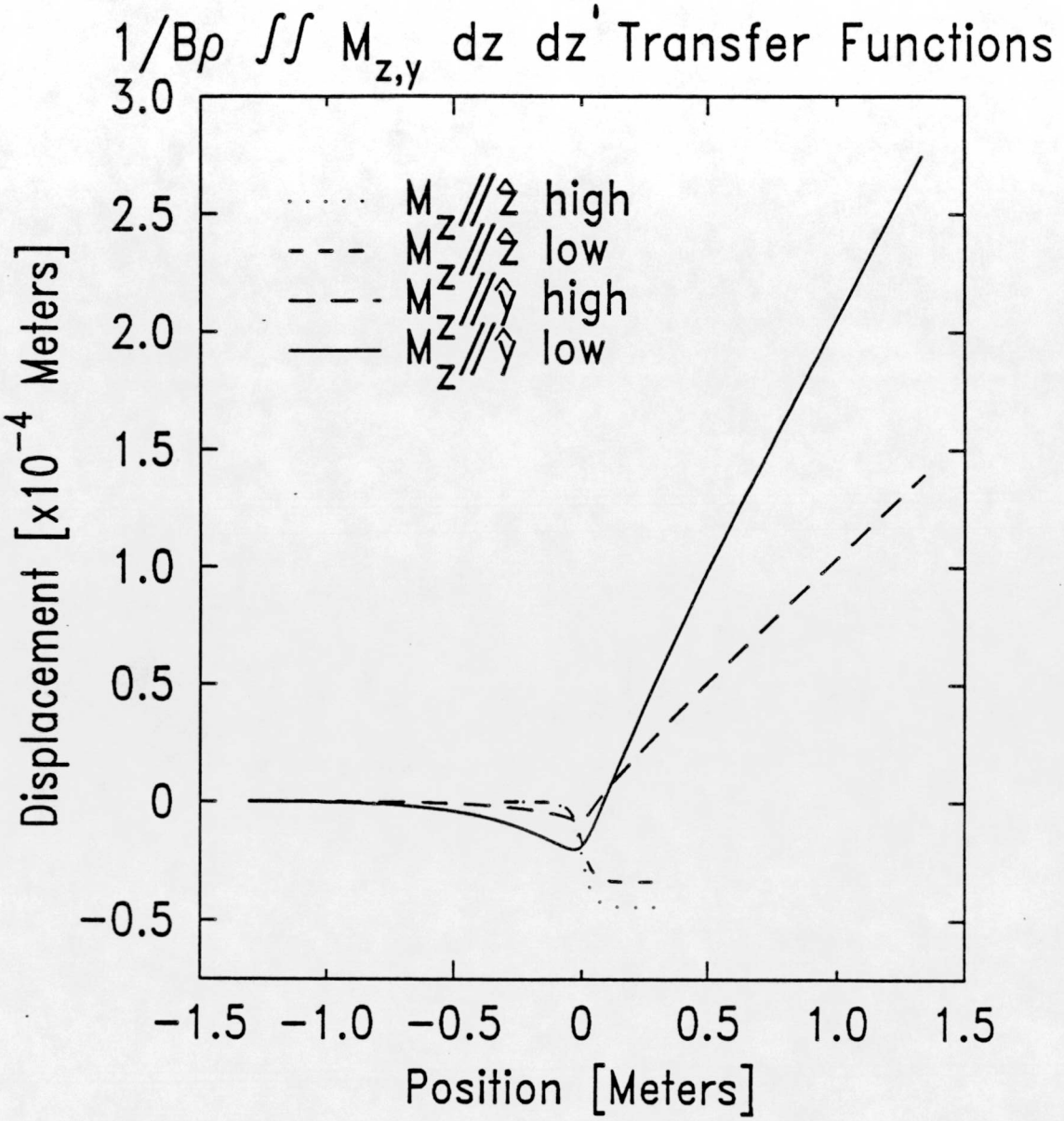

Figure 4 The second integral of the single block transfer functions of Figure 2.

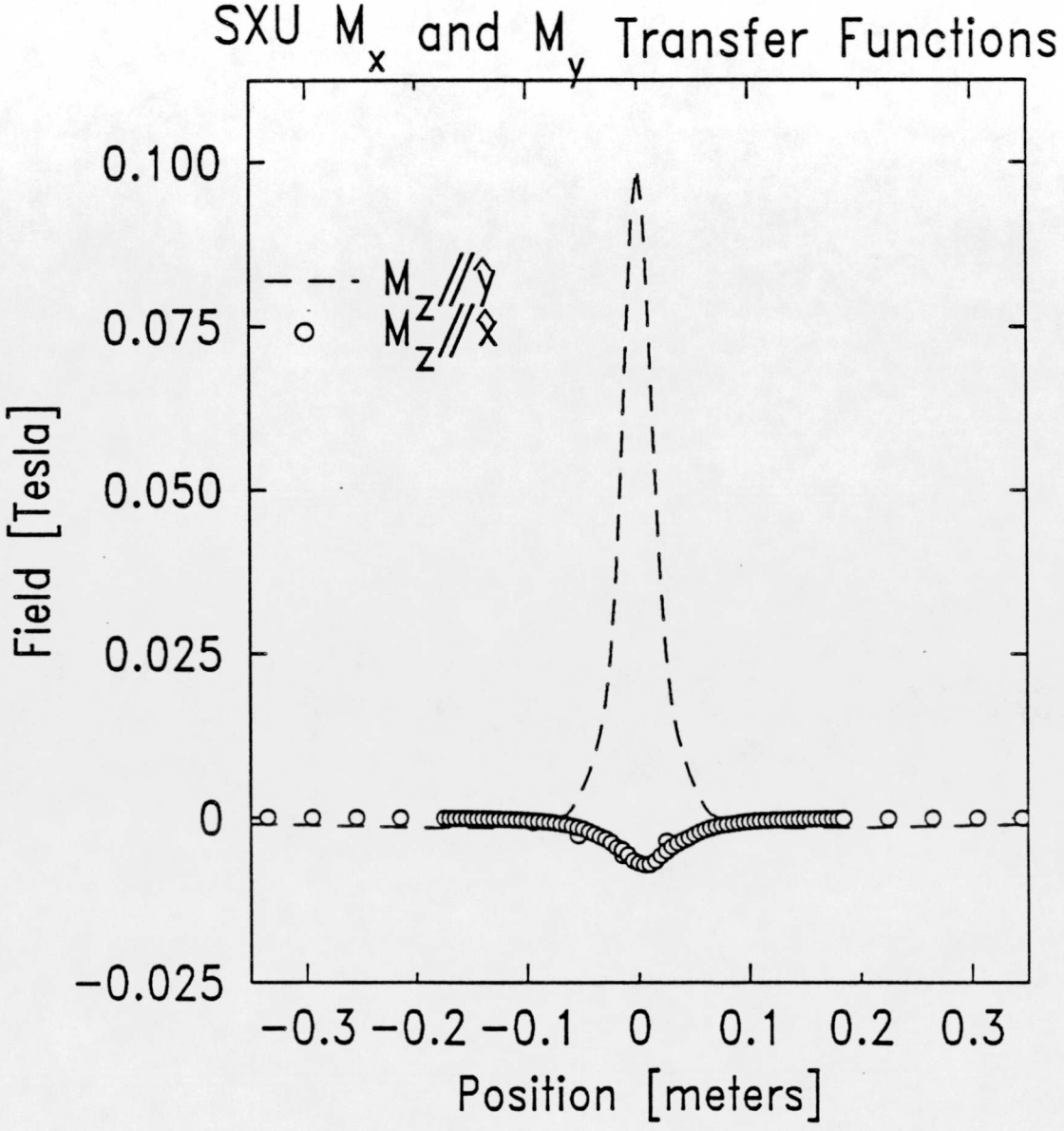

Figure 5 The transfer function of the two minor components of the magnet block i.e. M_z // to $\hat{y}$ and M_z // to $\hat{x}$.

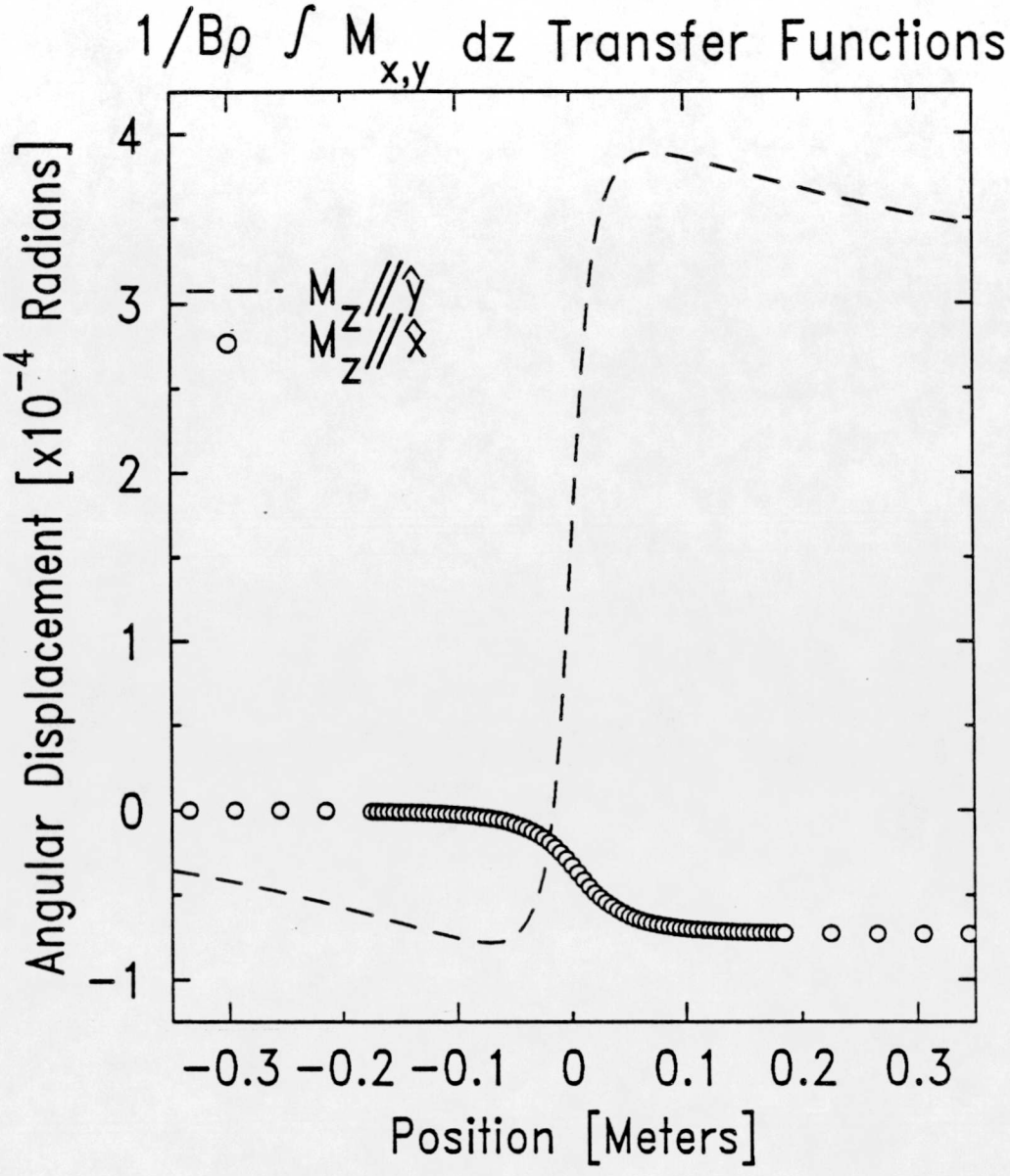

Figure 6 The first integral of the single block minor component transfer functions of Figure 5.

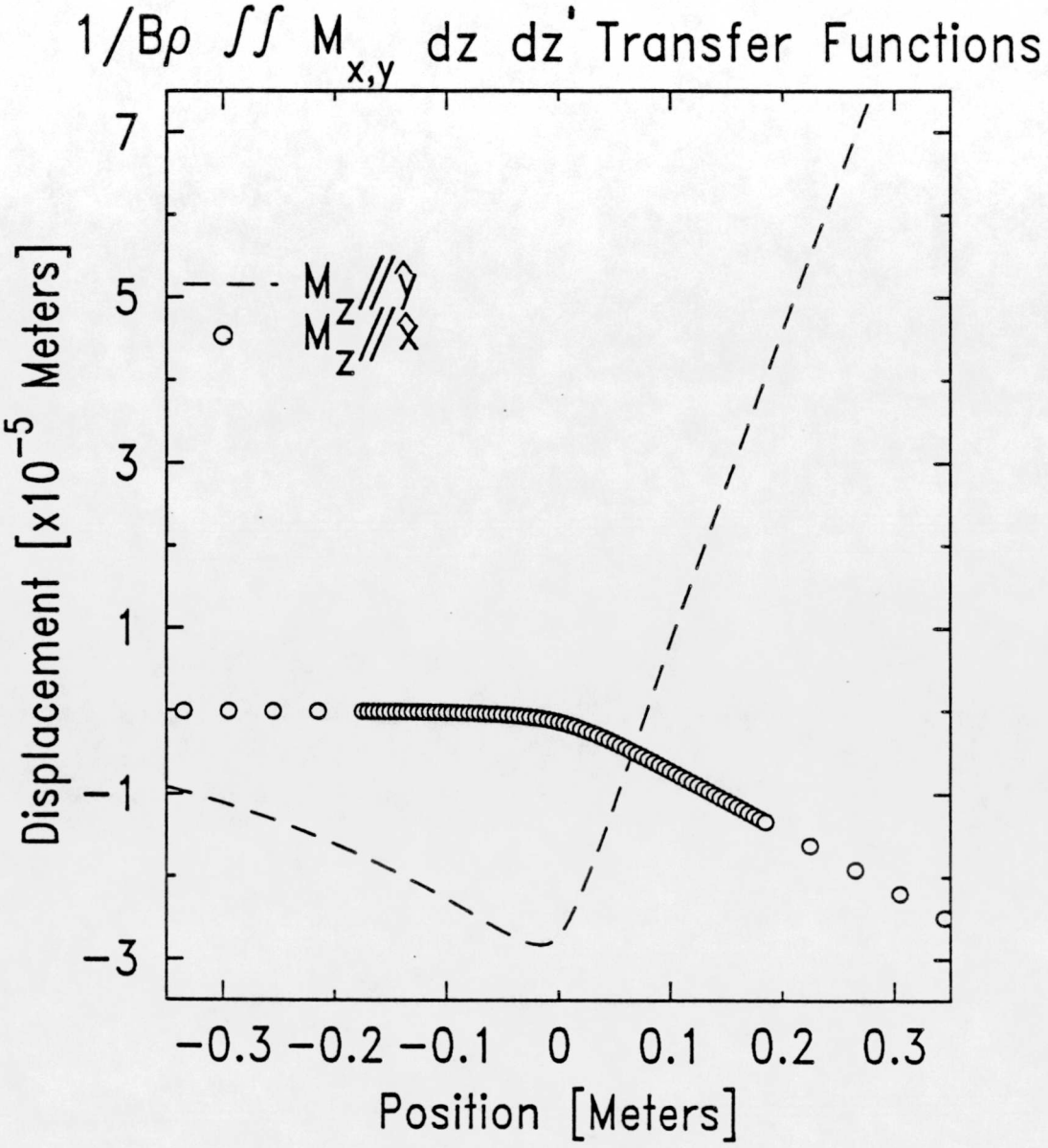

Figure 7 The second integral of the single block minor component transfer functions of Figure 5.

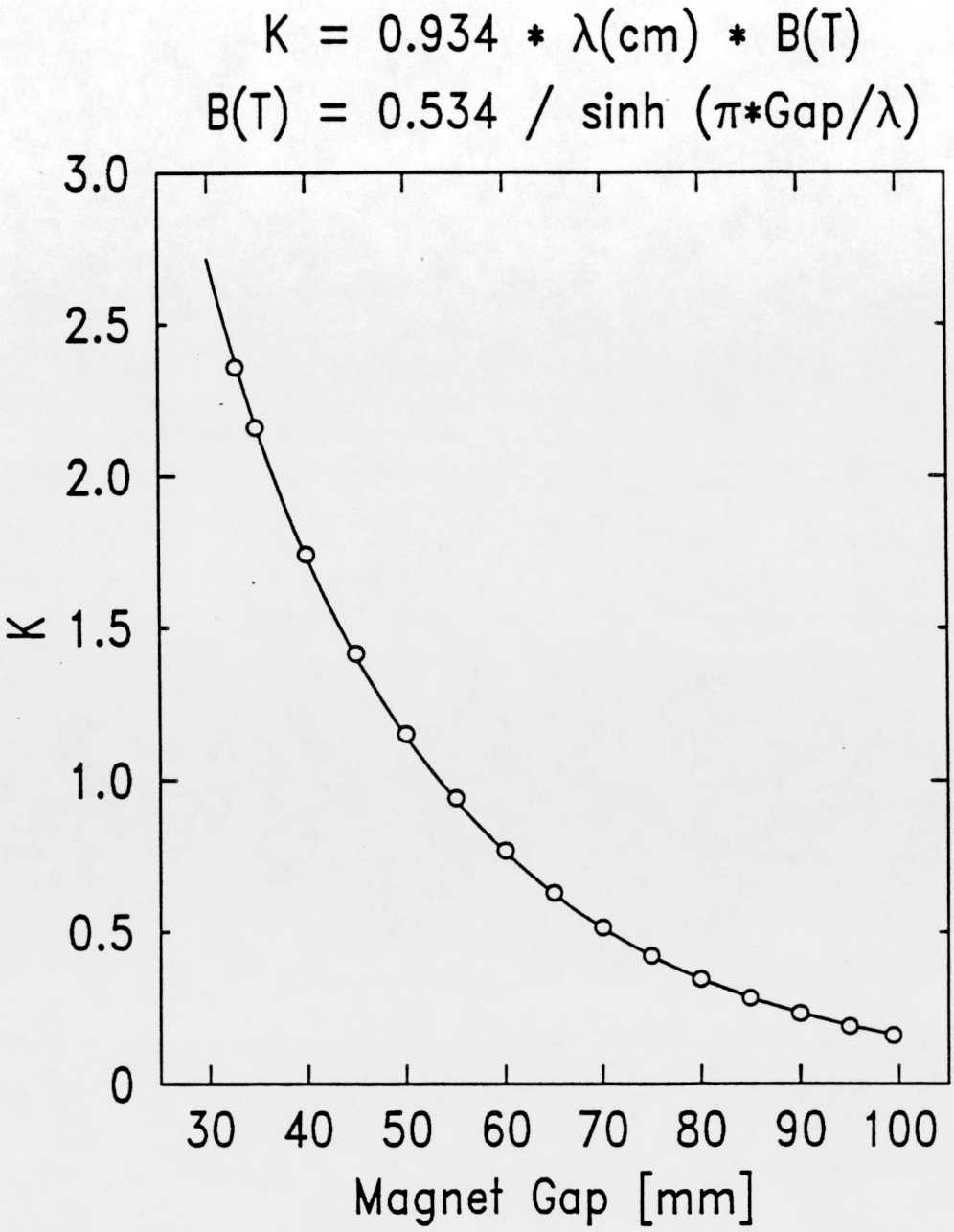

Figure 8 The undulator parameter K as a function of Gap

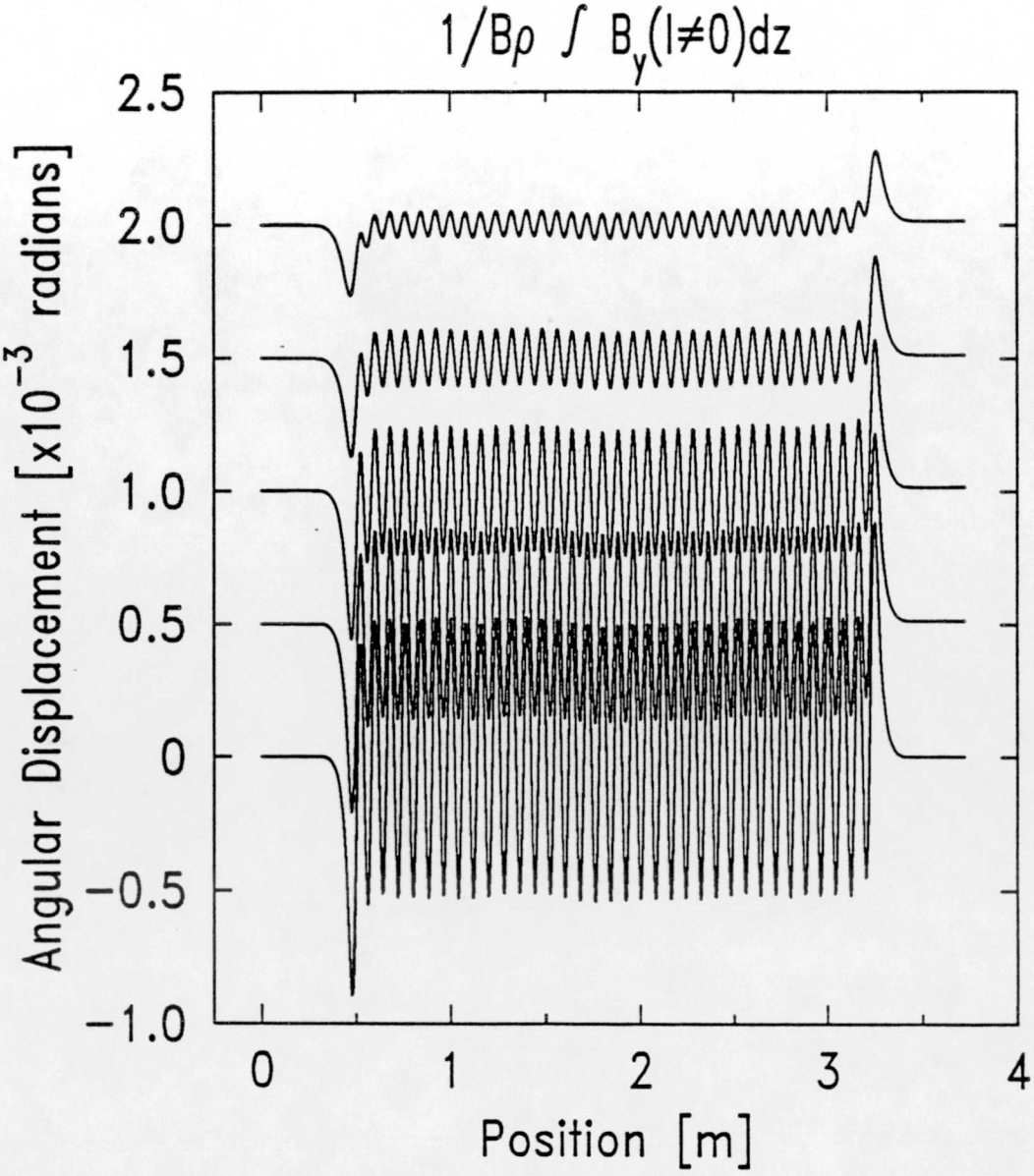

Figure 9 The magnetic field data at I=I_{oper} is integrated once to determine the angular displacement of the electron beam at magnet gaps of 90mm (I=-4.6amps), 70mm (I=-3.2amps), 50mm (I=-1.7amps), 40mm (I=-1.1amps), and 31mm (I=-0.65amps). For clarity the 40 mm trajectory is displaced by 0.5 $\times 10^{-3}$ radians from the 31 mm trajectory, the 50 mm trajectory is displaced by the same amount from the 40 mm trajectory, and so on.

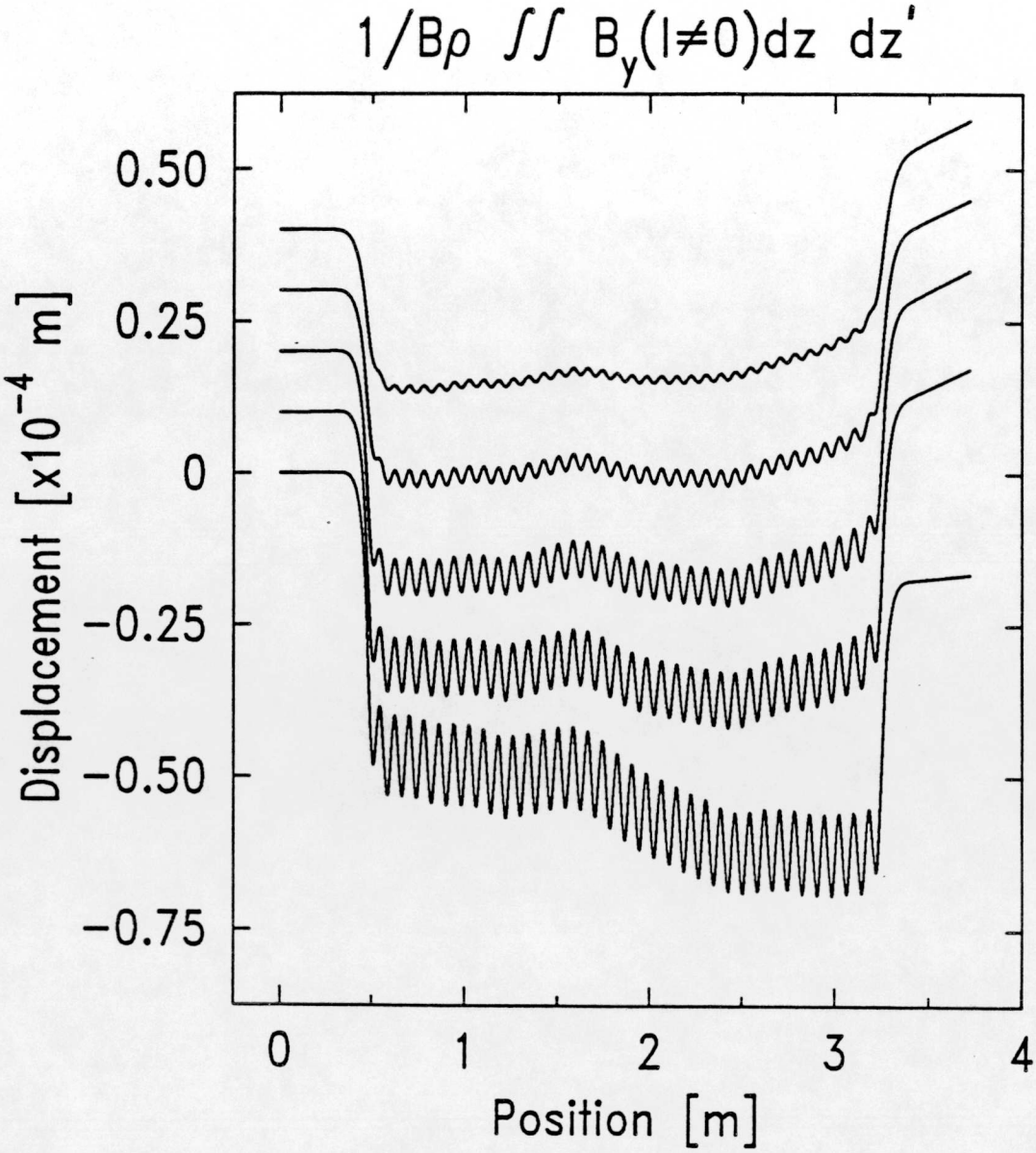

Figure 10 The magnetic field data at I=I_{oper} is integrated twice to determine the electron trajectory at magnet gaps of 90mm (I=-4.6amps), 70mm (I=-3.2amps), 50mm (I=-1.7amps), 40mm (I=-1.1amps), and 31mm (I=-0.65amps). For clarity, the 40 mm trajectory is displaced by 0.1 $\times 10^{-4}$ meters from the 31 mm trajectory, the 50 mm trajectory is displaced by the same amount from the 40 mm trajectory, and so on.

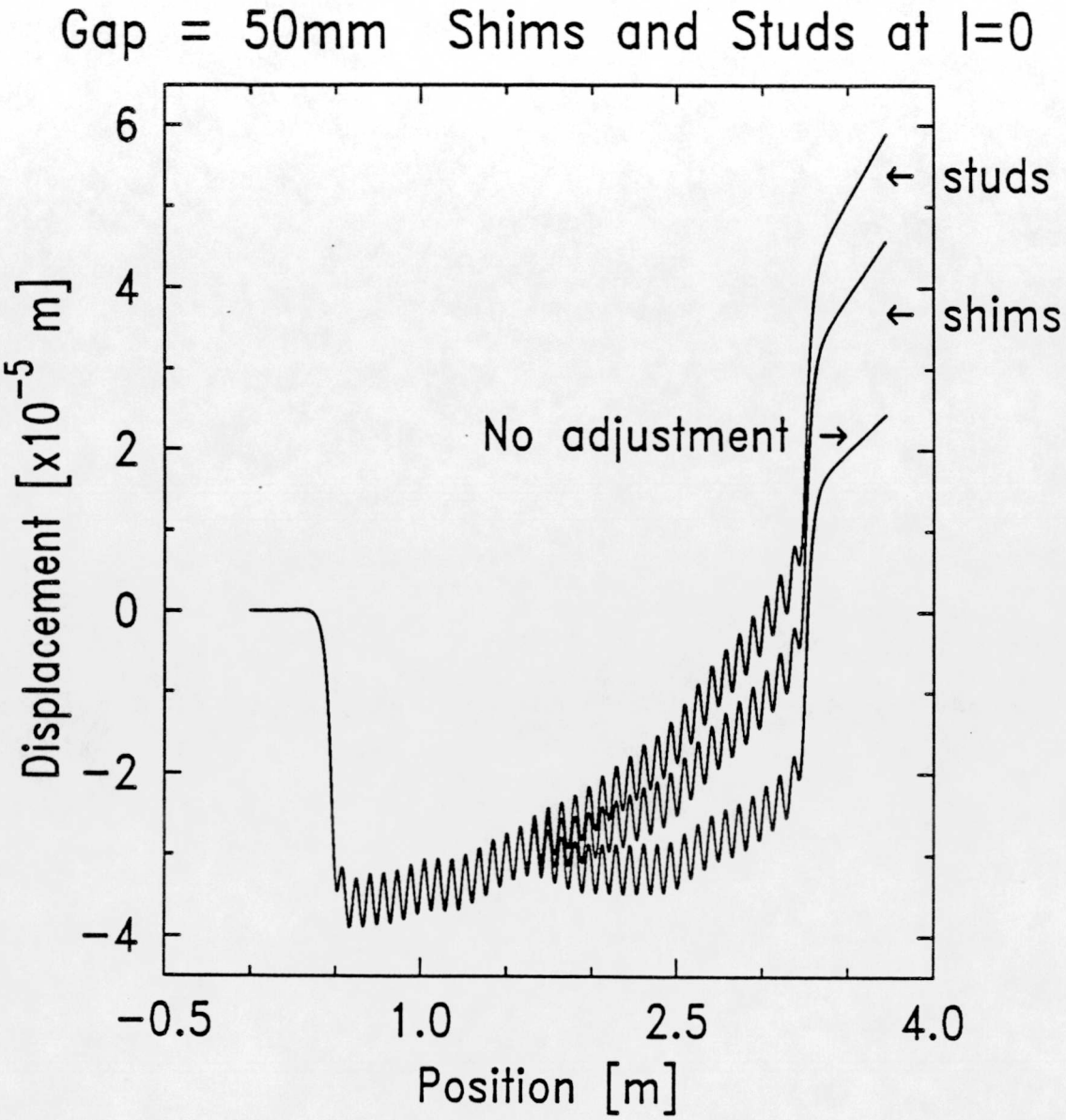

Figure 11 The effect of a 0.010" shim on poles 44 and 46, and the effect of a pole 45 stud, at a 50mm gap.

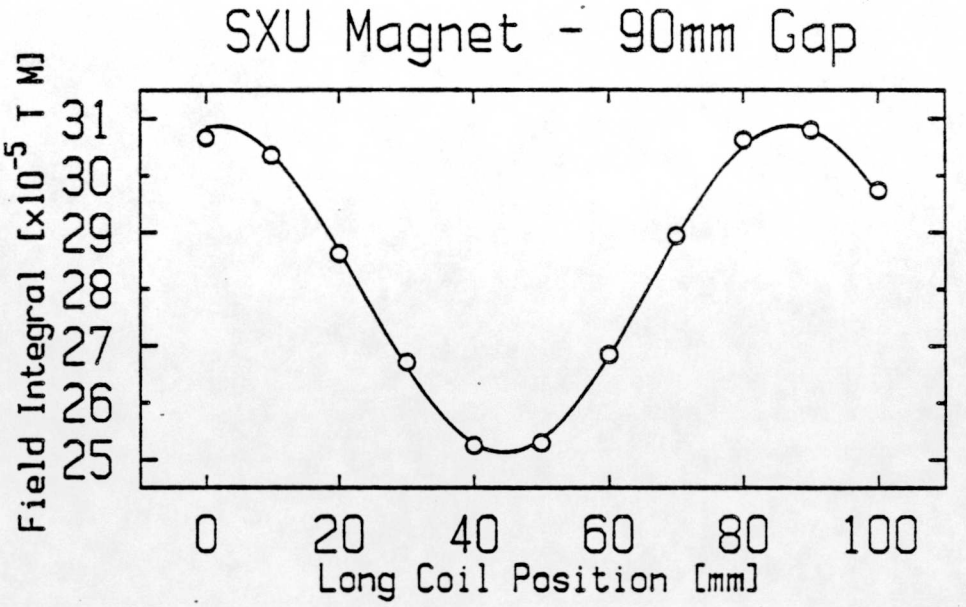

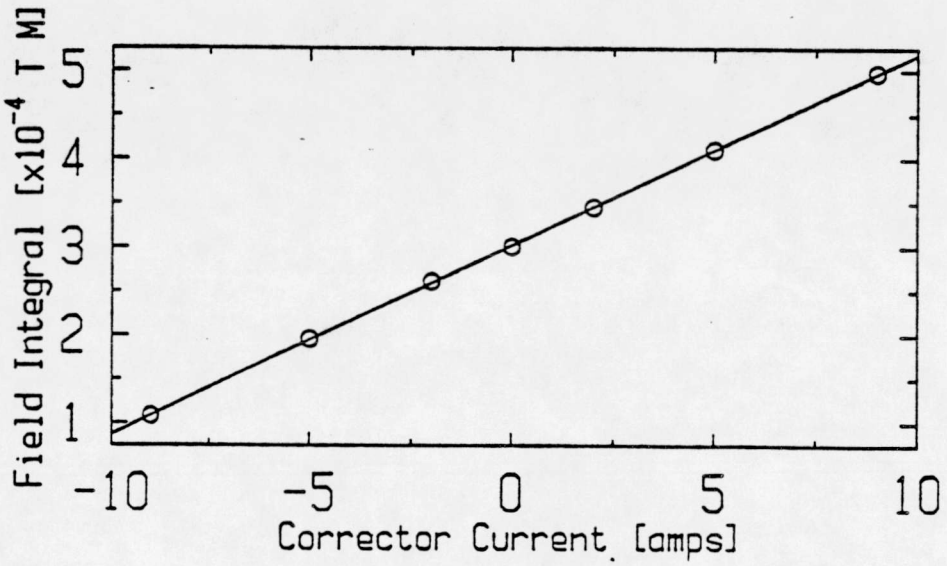

Figure 12 Top The long coil field integral plotted as a function of long coil position, fit to a sine wave.

Figure 12 Bottom The long coil field integral plotted as a function of corrector current, with a linear least squares fit.

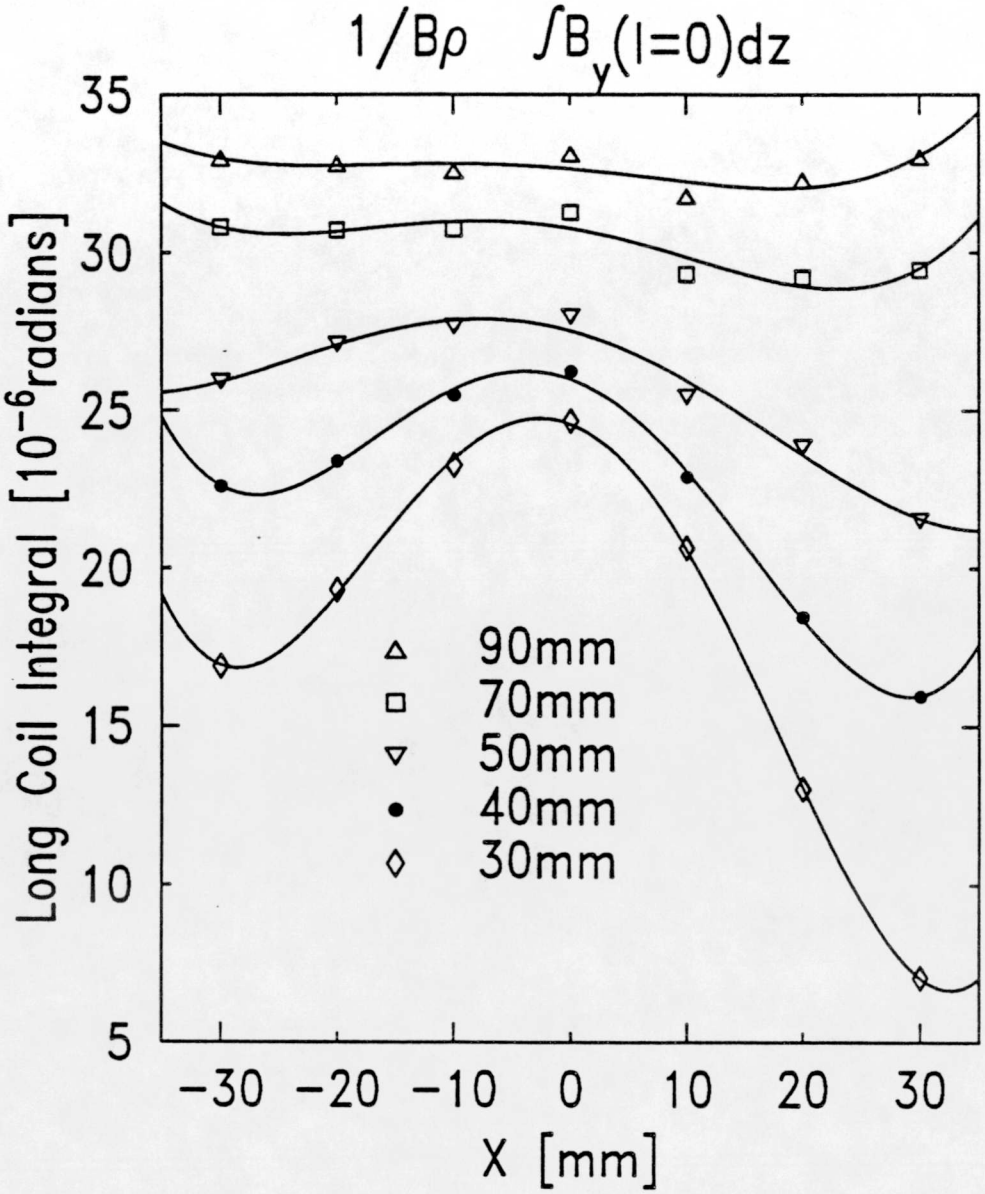

Figure 13 The long coil field integral at zero end corrector current, at 90, 70, 50, 40, and 31mm gaps as a function of X, with the fit to a fourth order polynomial indicated by the solid line.

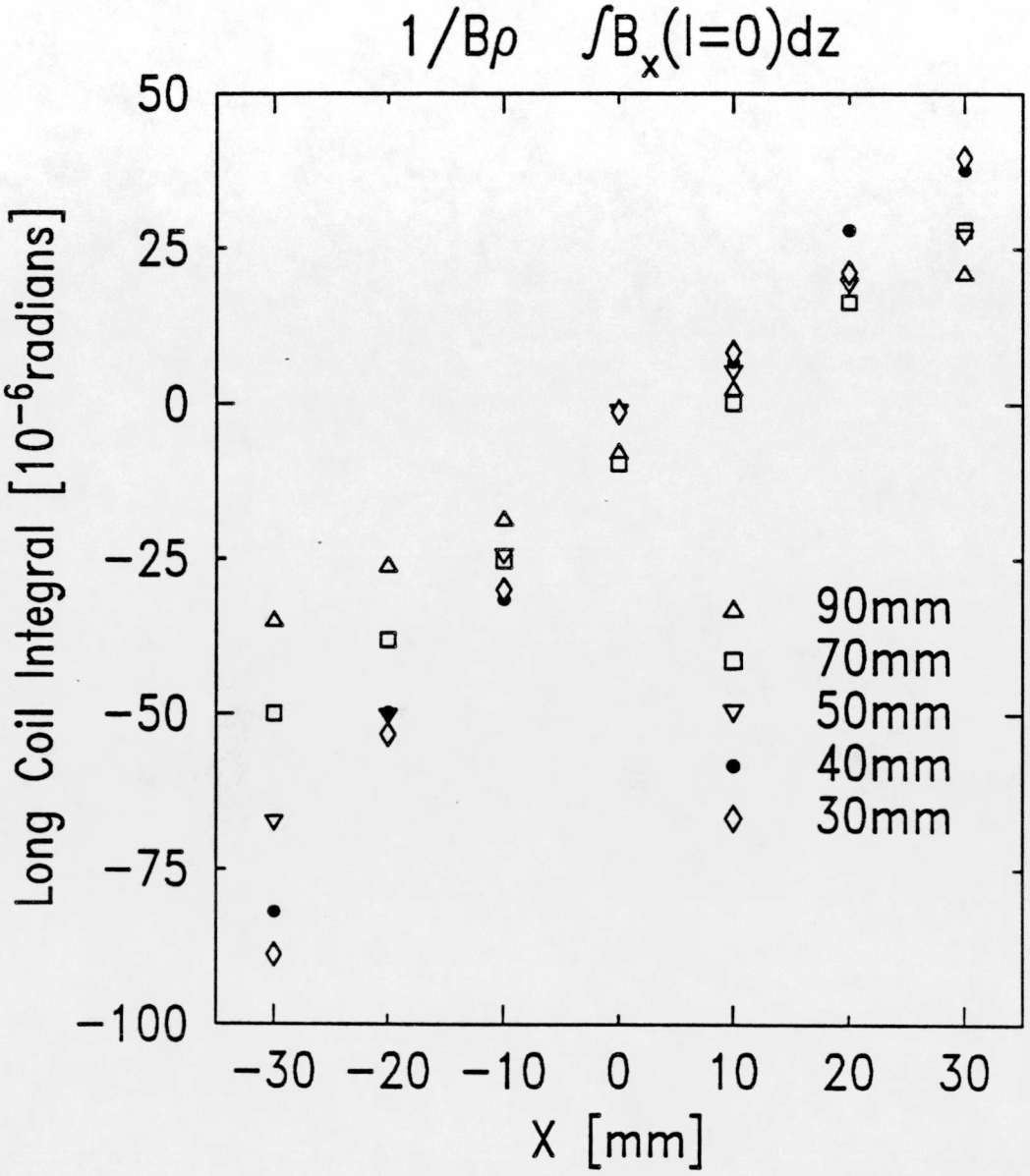

Figure 14 The long coil skew field integral at 90, 70, 50, 40, and 31mm gaps as a function of X.

List of Tables

	Long Coil Data on the SXU Magnet - Dipole Field Integral in units of 10^{-6} Radians				
	90mm Gap	70mm Gap	50mm Gap	40mm Gap	31mmGap
x= 30	33.00 + 2.198 × *I*	29.45 + 2.717 × *I*	21.51 + 3.505 × *I*	15.94 + 4.103 × *I*	7.053 + 4.790 × *I*
x= 20	32.27 + 2.394 × *I*	29.20 + 2.940 × *I*	23.84 + 3.754 × *I*	18.44 + 4.322 × *I*	13.01 + 5.026 × *I*
x= 10	31.77 + 2.507 × *I*	29.31 + 3.060 × *I*	25.44 + 3.856 × *I*	22.88 + 4.403 × *I*	20.62 + 5.085 × *I*
x= 0	33.10 + 2.544 × *I*	31.27 + 3.098 × *I*	27.98 + 3.880 × *I*	26.24 + 4.317 × *I*	24.67 + 5.085 × *I*
x=-10	32.56 + 2.509 × *I*	30.74 + 3.060 × *I*	27.68 + 3.854 × *I*	25.49 + 4.406 × *I*	23.27 + 5.081 × *I*
x=-20	32.79 + 2.400 × *I*	30.70 + 2.941 × *I*	27.10 + 3.747 × *I*	23.39 + 4.326 × *I*	19.31 + 5.018 × *I*
x=-30	32.97 + 2.213 × *I*	30.80 + 2.711 × *I*	25.92 + 3.484 × *I*	22.59 + 4.085 × *I*	16.89 + 4.758 × *I*

Table 1 The long coil dipole integrals measured for the SXU magnet as a function of transverse location X and end corrector current I.

Uncorrected multipoles in the SXU Magnet					
	Dipole	Quadrupole	Sextupole	Octupole	Decapole
	Tesla Meter	Tesla	Tesla/Meter	Tesla/Meter^2	Tesla/Meter^3
90	0.000272154	-0.000269093	-0.0239153	1.86233	410.854
70	0.000256468	-0.000508743	-0.0630512	2.196	691.418
50	0.000229536	-0.000831664	-0.1083370	1.515	508.654
40	0.000216706	-0.001114310	-0.2868820	1.26483	2167.37
31	0.000204846	-0.00118734	-0.446534	-1.24672	2843.56
Corrected multipoles in the SXU magnet					
	Dipole	Quadrupole	Sextupole	Octupole	Decapole
	Tesla Meter	Tesla	Tesla/Meter	Tesla/Meter^2	Tesla/Meter^3
90	0.000174552	-0.000266468	0.00418934	1.91666	420.91
70	0.000173838	-0.000506706	-0.044	2.16667	740
50	0.000180778	-0.000388135	-0.129015	-1.73333	752.727
40	0.000176661	-0.00111202	-0.289051	1.23167	2270.64
31	0.000177273	-0.00118776	-0.446674	-1.26667	2896.36

Table 2 Multipole analysis of the integrated dipole measurements as a function of transverse position X for both I=0.0 and I=I_{oper}.

	Long Coil Data on the SXU Magnet - Skew Dipole Field Integral in units of 10^{-6} Radians				
X(mm)	90mm Gap	70mm Gap	50mm Gap	40mm Gap	31mm Gap
x= 30	21.2	28.0	26.9	37.6	39.6
x= 20	21.2	16.4	19.1	28.0	21.2
x= 10	2.73	2.04	5.05	6.83	8.33
x= 0	-7.50	-9.56	-1.25		-1.23
x=-10	-18.4	-25.3	-24.6	-31.6	-30.0
x=-20	-25.9	-38.2	-50.5	-49.8	-53.3
x=-30	-34.8	-49.9	-67.6	-81.9	-88.8

Table 3 The long coil skew dipole integrals measured for the SXU magnet as a function of transverse location X.

Skew multipoles in the SXU Magnet			
Gap	Dipole	Quadrupole	Sextupole
(mm)	Tesla Meter	Tesla	Tesla/Meter
90	-0.000052	0.008	0.018
70	-0.000095	0.011	0.007
50	-0.000055	0.013	-0.28
40	-0.000074	0.016	-0.22
31	-0.000054	0.017	-0.35

Table 4 Multipole analysis of the integrated skew dipole measurements.

SXU Dipole Field Integral in units of 10^{-6} Radians					
Gap	Chosen I_{oper}	Long Coil I	Long Coil $I=I_{oper}$	Hall Probe* I=0.0	Hall Probe* $I=I_{oper}$
31	-0.65	$24.67 + 5.085 \times I$	21.32		
40	-1.1	$26.24 + 4.317 \times I$	21.32		17.21
50	-1.7	$27.98 + 3.880 \times I$	21.32	24.57	18.71
70	-3.2	$31.27 + 3.098 \times I$	21.32	31.26	17.14
90	-4.6	$33.10 + 2.544 \times I$	21.32	28.77	18.20

* The Long Coil length is 4.331m, while hall probe data was taken over a length of 3.720m. Since the net integrals are on the order of that due to the earth's magnetic field, the integrated hall probe data has been multipled by 4.331/3.720 for normalization.

Table 5 Comparison of the Hall probe and the long coil results as a function of gap